

Anisotropic contribution to the van der Waals and the Casimir-Polder energies for CO₂ and CH₄ molecules near surfaces and thin films

Priyadarshini Thiyam,^{1,*} Prachi Parashar,^{2,3,†} K. V. Shajesh,^{2,‡} Clas Persson,^{1,4,5} Martin Schaden,⁶ Iver Brevik,⁷ Drew F. Parsons,⁸ Kimball A. Milton,³ Oleksandr I. Malyi,^{5,§} and Mathias Boström^{5,¶}

¹*Department of Materials Science and Engineering,
Royal Institute of Technology, SE-100 44 Stockholm, Sweden*

²*Department of Physics, Southern Illinois University-Carbondale, Carbondale, Illinois 62901 USA*

³*Homer L. Dodge Department of Physics and Astronomy,
University of Oklahoma, Norman, Oklahoma 73019, USA*

⁴*Department of Physics, University of Oslo, P. O. Box 1048 Blindern, NO-0316 Oslo, Norway*

⁵*Centre for Materials Science and Nanotechnology,
University of Oslo, P. O. Box 1048 Blindern, NO-0316 Oslo, Norway*

⁶*Department of Physics, Rutgers, The State University of New Jersey, Newark, New Jersey 07102, USA*

⁷*Department of Energy and Process Engineering,
Norwegian University of Science and Technology, NO-7491 Trondheim, Norway*

⁸*School of Engineering and IT, Murdoch University, 90 South St, Murdoch, WA 6150, Australia*

In order to understand why carbon dioxide (CO₂) and methane (CH₄) molecules interact differently with surfaces, we investigate the Casimir-Polder energy of a linearly polarizable CO₂ molecule and an isotropically polarizable CH₄ molecule in front of an atomically thin gold film and an amorphous silica slab. We quantitatively analyze how the anisotropy in the polarizability of the molecule influences the van der Waals contribution to the binding energy of the molecule.

PACS numbers: 34.20.Cf; 42.50.Lc; 71.15.Mb

I. INTRODUCTION

Underground geological structures, e.g. rocks, shales and depleted coal beds, may contain large fractions of the world's future fossil energy in the form of light natural gas like methane [1]. New production methods like hydraulic fracturing or fracking by CO₂ injection allow trapped hydrocarbons to be produced directly from tight source rocks such as shale gas and shale oil systems [2]. The reason that this method works may be partly due to the difference in electron affinities of the CO₂ and CH₄ molecules [3]. Much basic research focuses on molecular physisorption/chemisorption and meso-scale transport processes in nanostructured shales [4]. By understanding the underlying physical processes, the ultimate aim of such research is to realize a controlled displacement of methane (CH₄) by carbon dioxide (CO₂) in hydrofractured shale and other formations. The added benefit of such a process is the simultaneous sequestration of the CO₂ gas. CO₂ gas can be trapped from huge point sources like power plants before it gets released into the atmosphere, and can be conveniently processed and utilized for fracking purposes [5].

From previous studies [6, 7] which do not take anisotropy into account, we know that a CO₂ molecule and a CH₄ molecule adhere to surfaces with very similar

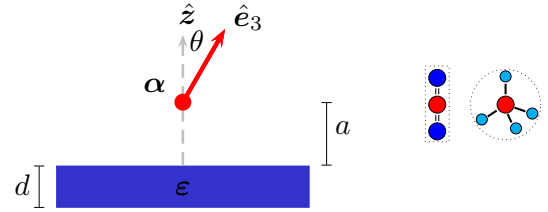


FIG. 1. (Color online) (Left) Schematic figure of an anisotropically polarizable molecule above a dielectric slab. (Right) Schematic figure showing anisotropy of CO₂ molecule and the isotropy of CH₄ molecule in their polarizabilities.

van der Waals energies while observed geological phenomena indicate strong preference of CO₂ molecule over CH₄ molecule in surface adsorption. In the present work, we explore the physical aspect of the underlying mechanism in order to understand the difference in interaction behavior of CO₂ and CH₄ molecules with surfaces with the focus being anisotropy in the electric polarizabilities of the respective molecules (see FIG. 1). We address this by studying the interaction energy of an anisotropically polarizable molecule in front of a dielectric slab of finite thickness which is anisotropic only in the direction perpendicular to the slab [8, 9]. We study the contribution from anisotropic polarizabilities to the Casimir-Polder interaction energy of a CO₂ and a CH₄ molecule in front of atomically thin gold films and an amorphous silica slab. We choose amorphous silica in particular because surfaces generated by hydraulic fracturing are mostly mineral surfaces like amorphous silica. Amorphous silica is isotropic in nature. We explore the data of the dielec-

* thiyam@kth.se

† prachi@nhn.ou.edu

‡ kvshajesh@gmail.com

§ oleksandr.malyi@smn.uio.no

¶ Mathias.Bostrom@smn.uio.no

tric function of gold available in Ref. [10] to study the variation of interaction energy with film thickness incorporating the effects of anisotropy of the gold film.

In the section II, we present the formalism of the Casimir-Polder interaction energy between a completely anisotropic molecule and a dielectric slab which is anisotropic in the direction perpendicular to the surface. In section III, we briefly summarize the method used for the calculation of the dielectric properties of the slabs. We also briefly describe the procedure used to obtain the anisotropic polarizabilities of the molecules. The dielectric functions of amorphous silica and gold are based on the density functional theory, and the anisotropic polarizabilities of CO₂ and CH₄ molecules are also obtained from ab initio calculations [11, 12]. Together the dielectric properties thus obtained are used to determine how the difference in the nature of polarizabilities of CO₂ and CH₄ distinguish their interaction energies. We present our results in section IV, and end with a few conclusions in section V.

II. FORMALISM

Consider an anisotropically polarizable molecule described by a frequency dependent molecular polarizability

$$\boldsymbol{\alpha}(\omega) = \alpha_1(\omega)\hat{\mathbf{e}}_1\hat{\mathbf{e}}_1 + \alpha_2(\omega)\hat{\mathbf{e}}_2\hat{\mathbf{e}}_2 + \alpha_3(\omega)\hat{\mathbf{e}}_3\hat{\mathbf{e}}_3, \quad (1)$$

at a distance a above an anisotropically polarizable dielectric slab of thickness d described by dielectric permittivity

$$\boldsymbol{\varepsilon}(\omega) = \varepsilon^\perp(\omega)\mathbf{1}_\perp + \varepsilon^\parallel(\omega)\hat{\mathbf{z}}\hat{\mathbf{z}}, \quad (2)$$

where \perp -components are in the x - y plane containing the dielectric slab and \parallel -component is normal to the surface of the slab. See FIG. 1. For an isotropic material like amorphous silica, we can set $\varepsilon^\perp = \varepsilon^\parallel$. Magnetic permeabilities for both the molecule and the dielectric slab are set to 1.

Here, the principal axes of the molecule are

$$\hat{\mathbf{e}}_1 = \cos\beta\hat{\boldsymbol{\theta}} + \sin\beta\hat{\boldsymbol{\phi}}, \quad (3a)$$

$$\hat{\mathbf{e}}_2 = -\sin\beta\hat{\boldsymbol{\theta}} + \cos\beta\hat{\boldsymbol{\phi}}, \quad (3b)$$

$$\hat{\mathbf{e}}_3 = \hat{\mathbf{r}}, \quad (3c)$$

where β is the rotation about the unit vector $\hat{\mathbf{e}}_3$, and $\hat{\mathbf{r}}$, $\hat{\boldsymbol{\theta}}$, and $\hat{\boldsymbol{\phi}}$ are the unit vectors in the spherical polar coordinates,

$$\hat{\mathbf{r}} = \sin\theta\cos\phi\hat{\mathbf{x}} + \sin\theta\sin\phi\hat{\mathbf{y}} + \cos\theta\hat{\mathbf{z}}, \quad (4a)$$

$$\hat{\boldsymbol{\theta}} = \cos\theta\cos\phi\hat{\mathbf{x}} + \cos\theta\sin\phi\hat{\mathbf{y}} - \sin\theta\hat{\mathbf{z}}, \quad (4b)$$

$$\hat{\boldsymbol{\phi}} = -\sin\phi\hat{\mathbf{x}} + \cos\phi\hat{\mathbf{y}}. \quad (4c)$$

Our configuration with an anisotropic molecule above a dielectric slab with isotropic polarizability in the x - y plane renders the interaction energy independent of ϕ . Thus, if necessary, one can choose $\phi = 0$, but we will not bother to do so. The Casimir-Polder interaction energy, in this case, at zero temperature in the Fourier transformed space is,

$$E = -\hbar c \int_{-\infty}^{\infty} \frac{d\zeta}{c} \int_0^{\infty} \frac{k_\perp dk_\perp}{2\pi} \int_0^{2\pi} \frac{d\phi_k}{2\pi} \frac{e^{-2\kappa a}}{2\kappa} I(i\zeta), \quad (5)$$

which is a generalization of the result given in Ref. [8]. The details of the derivation leading to Eq. (5) has been omitted for brevity. Here,

$$I(i\zeta) = r^H [\kappa^2(\hat{\mathbf{k}}_\perp \cdot \boldsymbol{\alpha} \cdot \hat{\mathbf{k}}_\perp) + k_\perp^2(\hat{\mathbf{z}} \cdot \boldsymbol{\alpha} \cdot \hat{\mathbf{z}})] - r^E \zeta^2 [(\hat{\mathbf{z}} \times \hat{\mathbf{k}}_\perp) \cdot \boldsymbol{\alpha} \cdot (\hat{\mathbf{z}} \times \hat{\mathbf{k}}_\perp)]. \quad (6)$$

The particular choice of $(\hat{\mathbf{k}}_\perp, \hat{\mathbf{z}} \times \hat{\mathbf{k}}_\perp, \hat{\mathbf{z}})$ basis facilitates separation of TM and TE modes. Specifically,

$$\hat{\mathbf{k}}_\perp = \cos\phi_k\hat{\mathbf{x}} + \sin\phi_k\hat{\mathbf{y}}, \quad (7a)$$

$$\hat{\mathbf{z}} \times \hat{\mathbf{k}}_\perp = -\sin\phi_k\hat{\mathbf{x}} + \cos\phi_k\hat{\mathbf{y}}. \quad (7b)$$

r^H and r^E are the reflection coefficients for TM- and TE-modes:

$$r^H = -\left(\frac{\bar{\kappa}^H - \kappa}{\bar{\kappa}^H + \kappa}\right) \frac{(1 - e^{-2\kappa^H d})}{\left[1 - \left(\frac{\bar{\kappa}^H - \kappa}{\bar{\kappa}^H + \kappa}\right)^2 e^{-2\kappa^H d}\right]}, \quad (8a)$$

$$r^E = -\left(\frac{\kappa^E - \bar{\kappa}}{\kappa^E + \bar{\kappa}}\right) \frac{(1 - e^{-2\kappa^E d})}{\left[1 - \left(\frac{\kappa^E - \bar{\kappa}}{\kappa^E + \bar{\kappa}}\right)^2 e^{-2\kappa^E d}\right]}, \quad (8b)$$

where

$$\kappa^H = \sqrt{k_\perp^2 \frac{\varepsilon^\perp}{\varepsilon^\parallel} + \frac{\zeta^2}{c^2} \varepsilon^\perp}, \quad \bar{\kappa}^H = \frac{\kappa^H}{\varepsilon^\perp}, \quad (9a)$$

$$\kappa^E = \sqrt{k_\perp^2 + \frac{\zeta^2}{c^2} \varepsilon^\perp}, \quad \bar{\kappa} = \sqrt{k_\perp^2 + \frac{\zeta^2}{c^2}}, \quad (9b)$$

and, d is the thickness of the dielectric slab. The interaction energy after performing the ϕ_k integration is

$$E = -\hbar c \int_{-\infty}^{\infty} \frac{d\zeta}{c} \int_0^{\infty} \frac{k_{\perp} dk_{\perp}}{2\pi} \frac{e^{-2\kappa a}}{2\kappa} \left\{ k_{\perp}^2 r^H \alpha_3 + \left(\frac{\zeta^2}{c^2} (r^H - r^E) + k_{\perp}^2 r^H \right) \left(\frac{\alpha_1 + \alpha_2}{2} \right) \right. \\ \left. + \frac{1}{2} \left(\frac{\zeta^2}{c^2} (r^H - r^E) - k_{\perp}^2 r^H \right) \left(\alpha_3 - \frac{\alpha_1 + \alpha_2}{2} + \left(\frac{\alpha_2 - \alpha_1}{2} \right) \cos 2\beta \right) \sin^2 \theta \right\}, \quad (10)$$

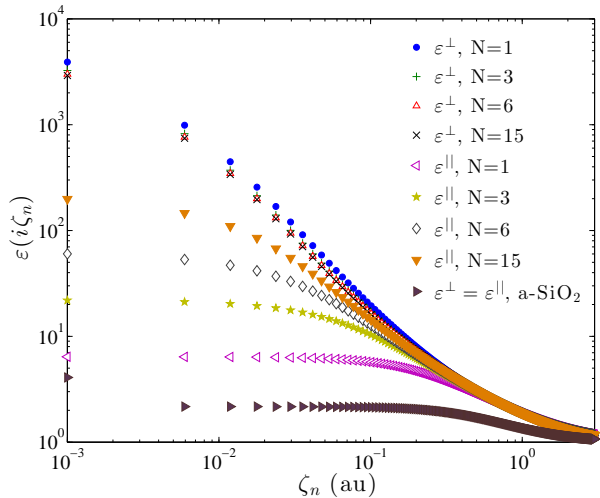


FIG. 2. (Color online) The perpendicular and parallel dielectric constants for $N=1, 3, 6$ and 15 atomic layers of gold, and for an amorphous silica slab (written as a-SiO₂ in the figure) in terms of the Matsubara frequencies. The perpendicular components of the $3, 6$ and 15 atomic-layer thick gold films almost overlap. The dielectric constants at zero frequency are shown on the y -axis. $1 \text{ au} = 6.57968 \times 10^{15} \text{ Hz} = 27.212 \text{ eV}$.

where we have suppressed the frequency dependence. The orientation dependence appears only in the last term, which vanishes for $\theta = 0, \pi$.

$$E^{NR} = -2k_B T \sum_{n=0}^{\infty} \int_0^{\infty} dk_{\perp} k_{\perp}^2 \Delta e^{-2k_{\perp} a} \left\{ \alpha_3 + \left(\frac{\alpha_1 + \alpha_2}{2} \right) - \frac{1}{2} \left(\alpha_3 - \frac{\alpha_1 + \alpha_2}{2} + \left(\frac{\alpha_2 - \alpha_1}{2} \right) \cos 2\beta \right) \sin^2 \theta \right\}, \quad (13)$$

using $r^H \rightarrow \Delta = \frac{\varepsilon-1}{\varepsilon+1}$ and $r^E \rightarrow 0$. This energy is proportional to $\frac{1}{a^3}$.

A. Perfect conductor limit

In the perfect conductor static limit, when $r^H \rightarrow 1$ and $r^E \rightarrow -1$ and the molecular polarizability gets a contribution only from the zero frequency, we reproduce the known result for the Casimir-Polder energy between an anisotropic molecular and a perfectly conducting slab:

$$E = -\hbar c \frac{\alpha_1 + \alpha_2 + \alpha_3}{8\pi a^4}, \quad (11)$$

where last term in Eq. (10) uniformly integrates to zero. Thus in this case the orientation of the molecule has no effect on the interaction energy.

B. Temperature dependence

To account for the temperature (T) dependence, we simply replace the integration over imaginary frequencies by a summation over discrete Matsubara frequencies ζ_n [13, 14],

$$E = -2k_B T \sum_{n=0}^{\infty} \int_0^{\infty} dk_{\perp} k_{\perp} \frac{e^{-2\kappa a}}{2\kappa} I(i\zeta_n), \quad (12)$$

where $\zeta_n = 2\pi k_B T n / \hbar$, k_B is the Boltzmann constant, and the prime indicates that the $n = 0$ term should be divided by 2. $I(i\zeta_n)$ is given by Eq. (6), with ζ replaced by ζ_n .

C. Non-retarded limit

In the non-retarded limit $\zeta_n = 0$, the finite temperature interaction energy between an anisotropic molecule at a distance a above an isotropic half-space Eq. (10) turns out to be,

III. DIELECTRIC FUNCTION AND POLARIZABILITY

All calculations for amorphous silica were carried out using the Vienna ab initio simulation package (VASP)

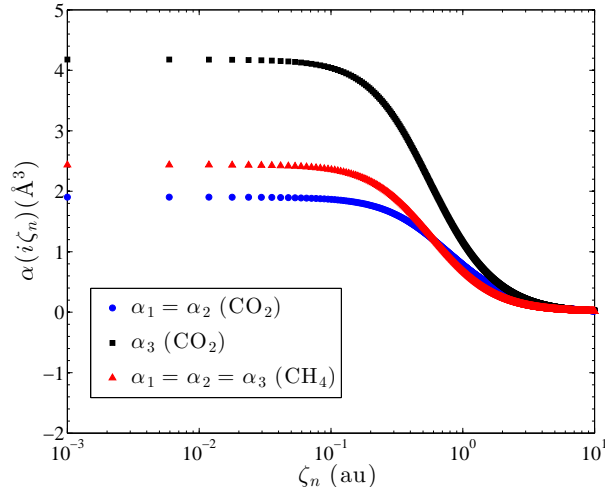


FIG. 3. (Color online) The anisotropic polarizabilities of CO_2 and CH_4 in units of \AA^3 in terms of the Matsubara frequencies. The zero frequency polarizabilities are indicated on the y -axis. Note that CO_2 is much more polarizable in the transverse direction.

with the Perdew-Burke-Ernzerhof (PBE) [15] functional. Projector augmented wave (PAW) pseudopotentials [16, 17] were used to model the effect of core electrons. The non-local parts of the pseudopotentials were treated in the real space for the Born-Oppenheimer molecular dynamics (BOMD) and in the reciprocal space for all other density functional theory (DFT) calculations. The structure of amorphous silica was generated using the BOMD simulations of 72-atom supercell with different annealing-quenching temperature protocols similar to earlier studies [18, 19]. The dielectric properties of amorphous silica were then calculated using the scissors-operator approximation ($\Delta=3.6$) for PBE calculations. The dielectric function on the imaginary frequency axis was determined using the Kramers-Kronig dispersion relation. The low-energy spectra are verified by calculating the static dielectric constants from the Born effective charges. The static dielectric constant was found to be 4.08 ± 0.11 . The details of the calculations of anisotropic dielectric functions for gold sheets were presented by Boström et al. in Ref. [10]. We plot the parallel and perpendicular dielectric constants as defined in Eq. (2) of different thicknesses of gold films, and of amorphous silica in FIG. 2.

The anisotropic polarizability tensors at imaginary frequencies for CO_2 and CH_4 were calculated using the quantum chemistry package MOLPRO [20]. Calculations were performed at the coupled clusters, singles and doubles (CCSD) level of theory. The correlation-consistent aug-cc-pVQZ basis set [21] was used. The geometries of the molecules were first optimized by energy minimization before being used in polarizability calculations. All calculations were done at room temperature. We show the anisotropic polarizabilities of CO_2 and CH_4 molecules in FIG. 3.

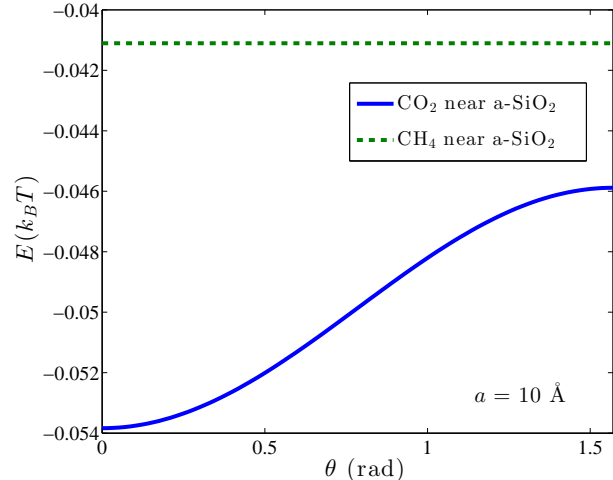


FIG. 4. (Color online) Comparing the interaction energy of CO_2 and CH_4 molecules at a distance of 10 \AA from an amorphous silica slab with respect to θ -orientation. We refer to the configuration $\theta = 0$ as the parallel orientation and $\theta = \pi/2$ as the perpendicular orientation. All energies are in units of $k_B T$.

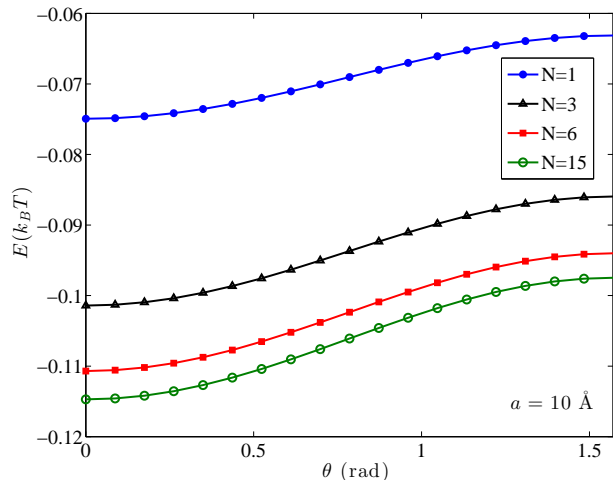


FIG. 5. (Color online) Interaction energy curves of a CO_2 molecule for different θ -orientations near gold films of N -atomic-layer thickness. The corresponding energies for a CH_4 molecule are -57.9 , -77.8 , -84.8 and -87.8 in units of $10^{-3} k_B T$ for $N=1$, 3 , 6 and 15 respectively.

IV. NUMERICAL RESULTS

For a linear molecule like CO_2 , the two most notable configurations are the parallel and perpendicular orientations with respect to the dielectric slab, and we are interested in the change in interaction energies in going from one orientation to the other. By parallel orientation, we refer to the configuration in which $\hat{\mathbf{e}}_3$ is aligned along $\hat{\mathbf{z}}$ while perpendicular orientation refers to the case

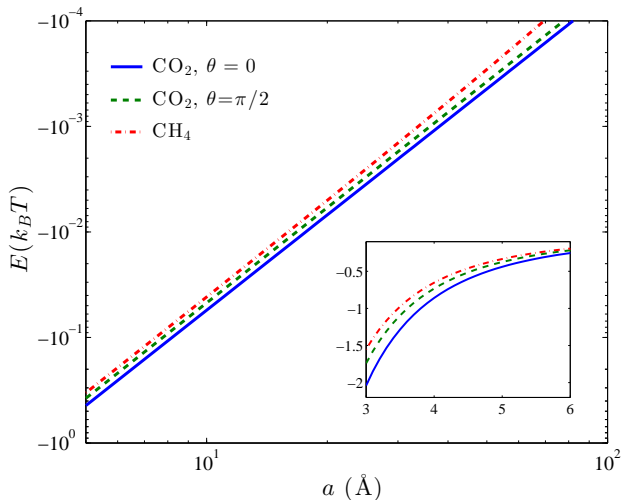


FIG. 6. (Color online) Comparing the interaction energy of CH_4 and CO_2 molecules at the parallel ($\theta = 0$) and the perpendicular ($\theta = \pi/2$) orientations at a varying distance from an amorphous silica slab. The interaction energy for a methane molecule is independent of θ -orientation. The inset figure shows the small distance limit. The axis labels and the legends of the outer figure hold for the inset figure as well.

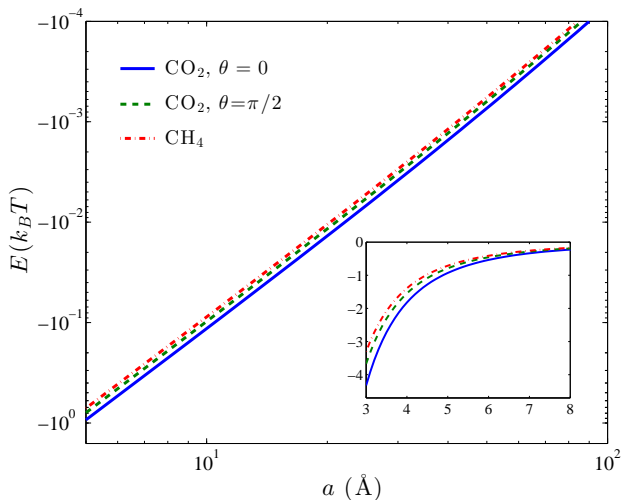


FIG. 7. (Color online) Comparing the interaction energy of CH_4 and CO_2 molecules at the parallel ($\theta = 0$) and the perpendicular ($\theta = \pi/2$) orientations at a varying distance from a 15-atomic-layer thick gold film.

when they make an angle $\theta = \pi/2$. A CO_2 molecule has anisotropy in one direction in its diagonal basis as shown in FIG. 3. Thus, choosing \hat{e}_3 along the unique linear axis of the molecule, it is obvious from Eq. (10) that there is no β dependent term in the interaction energy. In this particular choice of axes, the unique linear axis of the CO_2 molecule is perpendicular to the surface when $\theta = 0$ (parallel orientation) and parallel to the surface when $\theta = \pi/2$ (perpendicular orientation). The curves in FIG. 4

show the Casimir-Polder interaction energies of a CO_2 and a CH_4 molecule for different θ -orientations placed at a distance of 10 \AA from an amorphous silica slab. As expected, a methane molecule being highly isotropic shows no change in energy with change in θ . A CO_2 molecule, on the other hand, exhibits a slight change in the interaction energy at different orientations. The curve in FIG. 4 shows that the CO_2 molecule has lower energy at the parallel orientation ($\theta = 0$) than at the perpendicular orientation ($\theta = \pi/2$) near an amorphous silica slab. Thus, the molecule is most stable when its unique linear axis is aligned perpendicular to the slab. Irrespective of their orientations, the magnitude of the energy is larger for a CO_2 molecule than for a CH_4 molecule. This may play a role in the observed preferential adsorption of CO_2 over CH_4 molecules on surfaces. These interaction energies are, however, very small compared to $k_B T$. They become comparable when the molecule is very near the surface (see insets of FIGs. 6 and 7). It should be noted that the dielectric continuum picture of our model breaks down at the small distance limit (roughly below 100 \AA). A more rigorous quantum chemistry calculation will be required to take into account the effects due to surface, bonding, etc.

To make an estimate within our model, we calculate the energy of a system consisting of an amorphous silica slab with CO_2 molecules in the parallel orientation at, say, 8 \AA and CH_4 molecules at, say, 5 \AA from the slab mimicking the condition when the CO_2 gas is being injected. We then consider the reverse system when the CO_2 molecules are at 5 \AA and CH_4 molecules at 8 \AA . The difference in the interaction energies between the two configurations is $0.078 k_B T$, which is roughly 18 % compared to the energy in the first configuration. Thus, the second system with CO_2 near the surface is more favorable. As stated earlier, at such small separation distances there would be considerable contributions to the interaction energy from other effects.

In FIG. 5, we plot curves for the variation of molecule-surface interaction energy with respect to θ for a CO_2 molecule near gold films of different thicknesses. As can be observed from the figure, thicker films give larger magnitudes of interaction energies. Only the interaction energy with the 1-atomic-layer thick gold film displays appreciable difference in comparison with the energy curve for $N=15$ atomic-layer thick gold film while the interaction energies with the 3 and 6-atomic-layer thick gold films gradually approach that of 15-atomic-layer thick gold film. The energy corresponding to $N=15$ atomic layers of gold is largest in magnitude. From FIGs. 4 and 5, we can see that the trends of the energy curves are alike but the molecules have energies larger in magnitude for the more dielectric gold film compared to 100 \AA thick amorphous silica. We also provide the corresponding energies for a CH_4 molecule near gold films of varying thickness in the caption of FIG. 5. They are θ independent.

In FIG. 6, we fix the CO_2 molecule in the parallel and

perpendicular orientations and plot the interaction energy with respect to separation distance from the amorphous silica slab on a logarithmic scale. The energy curve for CH₄, which is orientation-independent, is also shown. A small difference in the energy curves for the parallel and perpendicular orientations is observed for a CO₂ molecule. The interaction energy is larger in magnitude for a CO₂ molecule than for a CH₄ molecule at all separation distances from the slab owing to greater polarizabilities of CO₂ molecule. The curves follow the $\frac{1}{a^3}$ dependence of the non-retarded approximation up to a separation distance of few Ångströms, and gradually deviates. The inset figure shows the interaction energy in the small molecule-slab separation distance limit (on a linear scale). FIG. 7 shows similar curves near a 15-atomic-layer thick gold film.

V. CONCLUSIONS

In this work, we presented a generalized expression for the interaction energy between a completely anisotropic molecule and a dielectric slab polarizable in the direction perpendicular to the surface. Applying this to the specific case of a linearly polarizable CO₂ molecule and an isotropically polarizable CH₄ molecule, we showed that the anisotropy influences the van der Waals energy to a small degree. The parallel orientation ($\theta = 0$) is more favored in comparison to the ($\theta = \pi/2$) perpendicular orientation in the case of a CO₂ molecule. In subsequent

studies, it will be interesting to incorporate the effects of finite-size of the molecule in which one has to carefully consider different radii of the anisotropic molecule in different directions for determination of the interaction energy for different orientations. In the future, we hope that it will prove possible to transcend the limitations of the continuum approximation, to get more reliable estimates of Casimir-Polder energies at very short distances than we can provide here.

ACKNOWLEDGEMENTS

PT gratefully acknowledges support from the European Commission; this publication reflects the views only of the authors, and the Commission cannot be held responsible for any use which may be made of the information contained therein. PT also acknowledges the Olle Eriksson's Foundation, Sweden (Grant: VT-2014-0001) for supporting a fruitful research visit at the Department of Physics, Southern Illinois University (SIU), Carbondale, USA. PT thanks SIU for hospitality. MB, OIM and CP acknowledge support from the Research Council of Norway (Project: 221469). CP acknowledges support from the Swedish Research Council (Contract No. C0485101). We acknowledge access to HPC resources at NSC through SNIC/SNAC and at USIT through NOTUR. The work of KAM is supported in part by a grant from the Julian Schwinger Foundation.

-
- [1] C. M. Oldenburg, K. Pruess and S. M. Benson, Process modeling of CO₂ injection into natural gas reservoirs for carbon sequestration and enhanced gas recovery, *Energy & Fuels* **15**, 293 (2001).
 - [2] Karim Sapag, Andrea Vallone, Andrés García Blanco and Cecilia Solar, *Adsorption of Methane in Porous Materials as the Basis for the Storage of Natural Gas*, in *Natural Gas* (2010), Primoz Potocnik (Ed.)
 - [3] R. Babarao, J. Jiang and S. I. Sandler, Molecular simulations for adsorptive separation of CO₂/CH₄ mixture in metal-exposed, catenated, and charged metal-organic frameworks, *Langmuir* **25**, 5239 (2008).
 - [4] H. Abdoulghafour, L. Luquot and P. Gouze, Characterization of the Mechanisms Controlling the Permeability Changes of Fractured Cements Flowed Through by CO₂-Rich Brine, *Environ. Sci. Technol.* **47**, 10332 (2013).
 - [5] R. Stuart Haszeldine, Carbon Capture and Storage: How Green Can Black Be?, *Science* **325**, 1647 (2009).
 - [6] P. Thiyam, C. Persson, B. E. Sernelius, D. F. Parsons, A. Malthé-Sørensen and M. Boström, Intermolecular Casimir-Polder forces in water and near surfaces, *Phys. Rev. E* **90**, 032122 (2014).
 - [7] P. Thiyam, C. Persson, D. F. Parsons, D. Huang, S. Y. Buhmann and M. Boström, Trends of CO₂ adsorption on cellulose due to van der Waals forces, *Colloids Surf. A: Physicochem. Eng. Aspects* **470**, 316 (2015).
 - [8] P. Parashar, K. A. Milton, K. V. Shajesh and M. Schaden, Electromagnetic semitransparent δ -function plate: Casimir interaction energy between parallel infinitesimally thin plates, *Phys. Rev. D* **86**, 085021 (2012) [arXiv:1206.0275 [hep-th]].
 - [9] K. V. Shajesh and M. Schaden, Repulsive long-range forces between anisotropic atoms and dielectrics, *Phys. Rev. A* **85**, 012523 (2012).
 - [10] M. Boström, C. Persson, and Bo E. Sernelius, Casimir Force between Atomically Thin Gold Films, *Eur. Phys. J. B* **86**, 43 (2013).
 - [11] D.F. Parsons and B. W. Ninham, Ab initio molar volumes and gaussian radii, *J. Phys. Chem. A* **113**, 1141 (2009).
 - [12] D.F. Parsons and B. W. Ninham, Importance of accurate dynamic polarizabilities for the ionic dispersion interactions of alkali halides, *Langmuir* **26**, 1816 (2009).
 - [13] E. M. Lifshitz, The theory of molecular attractive forces between solids, *Zh. Eksp. Teor. Fiz.* **29**, 94 (1955) [Sov. Phys. JETP **2**, 73 (1956)].
 - [14] J. Mahanty and B. W. Ninham, *Dispersion Forces* (Academic, London, 1976).
 - [15] J. P. Perdew, K. Burke and M. Ernzerhof, Generalized gradient approximation made simple, *Phys. Rev. Lett.* **77**, 3865 (1996).
 - [16] G. Kresse and D. Joubert, From ultrasoft pseudopotentials to the projector augmented-wave method, *Phys.*

- Rev. B **59**, 1758 (1999).
- [17] P. E. Blöchl, Projector augmented-wave method, Phys. Rev. B **50**, 17953 (1994).
- [18] J. Sarnthein, A. Pasquarello and R. Car, Structural and electronic properties of liquid and amorphous SiO₂: an ab initio molecular dynamics study, Phys. Rev. Lett. **74**, 4682 (1995).
- [19] R. M. Van Ginhoven, H. Jönsson and L. R. Corrales, Silica glass structure generation for ab initio calculations using small samples of amorphous silica, Phys. Rev. B **71**, 024208 (2005).
- [20] H.-J. Werner, P. J. Knowles, R. Lindh, F. R. Manby, M. Schütz, et al., *MOLPRO, version 2008.1, a package of ab initio programs*, (<http://www.molpro.net>, Cardiff, UK, 2008)
- [21] Kirk A. Peterson and Thom H. Dunning, Jr., Accurate correlation consistent basis sets for molecular core-valence correlation effects: The second row atoms Al-Ar, and the first row atoms B-Ne revisited, J. Chem. Phys. **117**, 10548 (2002).